BBA - Molecular Basis of Disease 1870 (2024) 167229

Contents lists available at ScienceDirect

BBA - Molecular Basis of Disease

journal homepage: www.elsevier.com/locate/bbadis

Integration of proteomic and metabolomic analysis reveal distinct metabolic alterations of prostate cancer-associated fibroblasts compared to normal fibroblasts from patient's stroma samples

Guillermo Bordanaba-Florit [a,*], Félix Royo [a,b], Oihane E. Albóniga [c], Aled Clayton [d], Juan Manuel Falcón-Pérez [a,b,c], Jason Webber [e,*]

[a] Exosomes Laboratory, Center for Cooperative Research in Biosciences (CIC bioGUNE), Derio, Spain
[b] Centro de Investigación Biomédica en Red de Enfermedades Hepáticas y Digestivas (Ciberehd), 28029 Madrid, Spain
[c] Metabolomics Platform, Center for Cooperative Research in Biosciences (CIC bioGUNE), Derio, Spain
[d] Division of Cancer and Genetics, School of Medicine, Cardiff University, Cardiff, UK
[e] Institute of Life Science, Swansea University Medical School, Swansea University, Swansea, UK

ARTICLE INFO

Keywords:
Mass spectrometry
Prostate cancer
Metabolism
Extracellular vesicles
Human primary fibroblasts

ABSTRACT

The prostate gland is a complex and heterogeneous organ composed of epithelium and stroma. Whilst many studies into prostate cancer focus on epithelium, the stroma is known to play a key role in disease with the emergence of a cancer-associated fibroblasts (CAF) phenotype associated upon disease progression. In this work, we studied the metabolic rewiring of stromal fibroblasts following differentiation to a cancer-associated, myofibroblast-like, phenotype. We determined that CAFs were metabolically more active compared to normal fibroblasts. This corresponded with a heightened lipogenic metabolism, as both reservoir species and building block compounds. Interestingly, lipid metabolism affects mitochondria functioning yet the mechanisms of lipid-mediated functions are unclear. Data showing oxidised fatty acids and glutathione system are elevated in CAFs, compared to normal fibroblasts, strengthens the hypothesis that increased metabolic activity is related to mitochondrial activity. This manuscript describes mechanisms responsible for the altered metabolic flux and shows that prostate cancer-derived extracellular vesicles can increase basal respiration in normal fibroblasts, mirroring that of the disease-like phenotype. This indicates that extracellular vesicles derived from prostate cancer cells may drive an altered oxygen-dependent metabolism associated to mitochondria in CAFs.

1. Introduction

The prostate gland is globally composed of epithelium and stroma, which are extremely heterogeneous tissues. The epithelium is organized as glandular acini and it contains cuboidal to columnar secretory epithelial cells with apical junction complexes, a continuous layer of basal cells [1], and sparse neuroendocrine cells, each attached to a basal lamina [2]. Beyond the basal lamina, a prominent fibromuscular stroma composed of smooth muscle, fibroblasts, blood vessels, autonomic nerve fibres, inflammatory cells, and extracellular matrix components offers physical support and contraction of the gland [3]. In prostate carcinoma (PCa), the interstitial stroma is often abnormally rich in myofibroblast-likecells [4,5], capable of supporting tumour growth, vascularization, angiogenesis, and metastasis *in vivo* [6]. Transforming growth factor β1, TGF-β1, remains among the most critical factors for fibroblast differentiation and the generation of a tumour reactive stroma. Intriguingly, we have previously shown that cancer extracellular vesicles (EVs) can trigger fibroblast to myofibroblast differentiation in an EV-TGF-β1

Abbreviations: 2-DG, 2-deoxy-D-glucose; *α-SMA*, α smooth muscle actin; *ATP*, Adenosine triphosphate; *CAF*, Cancer-associated fibroblast; *CE*, Cholesteryl ester; *Cer*, Ceramides; *ECAR*, Extracellular acidification rate; *EV*, Extracellular vesicle; *FA*, Fatty acid; *FCCP*, Carbonyl cyanide p-trifluoro methoxyphenylhydrazone; *FFAox*, Oxydised fatty acis; *GSH*, Glutathione; *HEPE*, Hydroxyeicosapentanoic acid; *LC-MS*, Liquid chromatography coupled to mass spectrometry; *LPC*, Lysophosphatidylcholines; *LPE*, Glycerophosphocholines; *MSI*, Mass spectrometry imaging; *NAD*, Nicotinamide adenine dinucleotide; *NAE*, N-acyl ethanolamines; *OCR*, Oxygen consumption rate; *PCa*, Prostate cancer; *PCA*, Principal component analysis; *PBS*, Phosphate buffered saline; *ROS*, Reactive oxygen species; *SEM*, Standard error of the mean; *TCA*, Tricarboxylic acid; *TGF-β1*, Transforming growth factor beta 1; *UPLC-MS*, Ultra-high performance liquid chromatography coupled to mass spectrometry.

* Corresponding authors.
E-mail addresses: gbordanaba@cicbiogune.es (G. Bordanaba-Florit), j.p.webber@swansea.ac.uk (J. Webber).

https://doi.org/10.1016/j.bbadis.2024.167229
Received 27 November 2023; Received in revised form 25 April 2024; Accepted 6 May 2024
Available online 10 May 2024

dependent manner [6]. In further studies, the essential role of EVs in directing this stromal cell differentiation towards cancer-associated myofibroblast-like phenotype was described [7]. However, the mechanisms by which EV-activated stromal cells support tumour growth remain unclear.

Our previous studies comparing stromal cells, from patient-derived biopsy material, revealed clear differences between normal and disease-associated stromal fibroblasts [8]. A panel of antibody markers confirmed the higher abundance of α-Smooth Muscle Actin (α-SMA)-positive myofibroblast cells in tumour-associated tissue. Strikingly, EVs isolated from prostate cancer epithelial cell lines were shown to trigger differentiation of normal fibroblasts to a myofibroblast-like phenotype, with pro-angiogenic function and capable of supporting tumour growth *in vivo* [7]. Further proteomics-based analysis highlighted that stroma activation mediated by EV stimulation mirrors the naturally occurring CAF phenotype observed during disease [8].

Altered metabolism is a hallmark of PCa and several metabolites and metabolic pathways are already distinctive in different prostate types of tissue [9,10]. Higher levels of energy-related pathway metabolites, such as ADP, ATP, and glucose as well as higher levels of the antioxidant taurine have previously been reported in stromal tissue compared to cancer and non-cancer epithelium [11]. Additional crucial metabolites for fatty acid oxidation and building blocks in lipid synthesis are known to be elevated in cancer compared to normal tissue. Other studies also reported metabolic rewiring of reactive stroma, showing different levels of certain metabolites between highly differentiated stroma compared to poorly differentiated stroma [12]. The stromal-epithelial interactions have a dominant role in tumour growth, invasion and metastasis. Actually, many reports over the last decades showed the interaction of reactive stroma with PCa [2,12–17] and EVs influencing aspects of cancer biology such as angiogenesis [7,8,18,19] and tumour progression [17,20–22]. Yet, few studies have investigated the role of tumour EVs in altering metabolic processes in stromal cell compartments.

With the rise of *omics* era, entire sets of biomolecules - genes, proteins or metabolites - contained in a biological tissue, cell, fluid, or organism can be identified. We have previously conducted a proteomic analysis of patient matched normal and cancer-associated stromal fibroblasts, revealing distinct differences between the two cell types [8] and have supported this with an analysis of RNA from stromal cells and their EVs [23]. This manuscript presents a broad semitargeted metabolomics approach that analyses the metabolome of these normal and disease-associated stromal fibroblasts from individual PCa patients. Metabolic differences related to lipogenic pathways and mitochondrial metabolism between these two fibroblast populations have been described. Furthermore, we explored how prostate-cancer derived EVs affect the metabolism of normal fibroblasts towards CAF-like phenotype.

2. Materials and methods

2.1. Stromal primary cell cultures

Six patient-matched normal and tumour-associated stromal cell lines were isolated from needle biopsies of radical retropubic prostatectomy cores, taken from apparently normal areas and sites of palpable disease from the same prostate. All patients who underwent prostatectomy were diagnosed with low-risk localised PCa (Gleason score 6). Representative cores underwent H&E staining, and confirmed as normal or cancer-associated stroma by an independent pathologist. Tissue collection and consenting was managed through the Wales Cancer Bank. Cores were manually dissected into $1mm^3$ pieces and subjected to mechanical homogenization followed by 200 U per mL collagenase-I digestion for 15 to 20 h at 37 °C. Cells were cultured in Stromal Cell Basal Medium (SCBM) supplemented with human fibroblast growth factor-B, insulin, fetal bovine serum (FBS) and GA-1000 (Lonza, Wokingham, UK) for around two weeks until only stromal cells were retained [8,23]. Subsequent cultures were maintained in DMEM/F12 media (Lonza) with 10 % FBS depleted of bovine EVs. Upon isolation of stromal fibroblasts, robust characterisation was performed including immuno-fluorescent visualisation of key markers Vimentin, Desmin, Cytokeratins 5 and 8, and α-SMA, as previously reported, to confirm cell phenotype [7,8]. Cultures were confirmed free of epithelial cells by immuno-fluorescence staining for Cytokeratins 5 and 8 prior seeding stromal cells in 96 well plates [8,23]. A sample of each patient-matched prostatic stromal cell culture was collected and frozen for metabolomics analysis using liquid chromatography coupled to mass spectrometry.

2.2. Metabolite extraction

In metabolomics, there is no single platform or method able to analyse the entire metabolome of a biological sample. Therefore, metabolites were extracted by fractionating the cell samples into pools of species with similar physicochemical properties. In brief, proteins were precipitated by adding methanol to the cell lysate. Chloroform solvent was added to the methanol extraction mixture and this biphasic mixture was incubated at −20 °C for 30 min. Then, three different fractions were collected: (1) fatty acyls, bile acids, steroids and lysoglycerophospholipids (Platform 1), were obtained after centrifuging the supernatant at 16,000*g* for 15 min, drying and reconstituting in methanol, (2) for aminoacids (Platform 3), aliquots of 5 μL from Platform 1 were derivatised and dried, and (3) glycerolipids, cholesteryl esters, sphingolipids and glycerophospholipids (Platform 2) were obtained by mixing the chloroform extraction mixture with H_2O (pH 9) and incubating at −20 °C for 60 min. After centrifuging at 16,000*g* for 15 min, the organic phase from this third fraction was collected then, dried and reconstituted in 50/50 % *v/v* acetronitrile/isopropanol. The aqueous phase that contains polar metabolites, including central carbon metabolism (Platform 4), was collected, dried and reconstituted in H_2O.

Quality control (QC) sample for calibration and validation were included in this workflow to correct for response factors between and within batches; and to assess the quality of data.

2.3. LC-MS analysis

An appropriate UPLC-MS method was used for each platform. The instruments and the conditions for the chromatographic separation and mass spectrometric detection are summarized in Table S1. A test mixture of standard was analysed before and after the entire set of randomized, duplicated sample injections to check for retention time stability, mass accuracy and sensitivity. All data were processed using the TargetLynx application manager for MassLynx 4.1 software (Waters Corp., Milford, USA). A set of predefined features, defined as retention time - mass-to-charge ratio pairs, *Rt-m/z*, corresponding to metabolites included in the analysis are fed into the program. Associated extracted ion chromatograms (mass tolerance window = 0.05 Da) are then peak-detected and noise-reduced in both the LC and MS domains such that only true metabolite related features are processed by the software. Then, a list of chromatographic peak areas is generated for each sample injection.

2.4. Data analysis

2.4.1. Data Normalization and quality control

After data inspection in terms of reproducibility and peak integration, each metabolite was corrected and normalized using the intensity of an appropriate internal standard included in the analysis and following the procedure fully described by van der Kloet et al. [25] Finally, any remaining zero values in the corrected dataset were replaced with missing values prior averaging to obtain a dataset further used for statistical analyses. A final normalization procedure was applied by dividing every sample by its protein content.

2.5. Multivariate and univariate analysis

Once data was normalized and prepare for statistical analysis a first approach based on multivariate analysis was performed with SIMCA-P (version 13.0). Firstly, a non-supervised principal component analysis (PCA) was used to reduce dimensionality and to study data quality, assess reproducibility of the analytical procedure, visualise tendencies between groups and determine the presence of outliers. A comprehensive evaluation of data showed a clear tendency of enhanced abundances in most of the metabolites in sample normal stroma-1161 during data analysis and normalization compared to other patient-matched tissues. PCA (Fig. S1) also shows that this sample is distinct from the five remaining paired samples and, a confidence ellipse produced using Hotelling's T2 (significance level = 0.05) confirms this. For these reasons, this sample was excluded from further statistical analysis. Afterwards, supervised partial least squares discriminant analysis (PLS-DA) and/or orthogonal PLS-DA (OPLS-DA) were performed followed by a suitable validation method by cross-validation analysis of variance (CV-ANOVA) integrated in SIMCA-P software. Then, supervised models were used for variable selection. In this sense, a variable importance on projection (VIP) score and absolute value of p(corr) >1 and 0.8, respectively, were used as cut-off points for variable selection.

Finally, and as a complementary statistical analysis, univariate analysis was perfomed. In order to test normality, Shaphiro test was used; thence either paired student's test [26] or Wilcoxon signed-rank test was applied to assess comparisons significance. After that, the dataset was expressed as a metabolite fold-change and significance (*p*-value) and further depicted in a *volcano plot*.

2.6. Pathway analysis and pathway enrichment

A proper biological interpretation is crucial in any metabolomics study to deliver a comprehensive assessment of experimental conditions. To evaluate the prominence of certain metabolic pathways, a Pathway analysis was computed using MetaboAnalyst 5.0 and inputting a dataset of samples and quantified metabolites. It performs an o-representation analysis that integrates enrichment and pathway topology analysis to visualise specific altered pathways in the human metabolic network [27]. Then, proteomics data was included in a Joint-pathway analysis to evaluate metabolic alterations considering two sets of physiologically relevant molecules in fibroblast samples. This over-representation analysis module performs an integrated metabolic pathway analysis by combining metabolomics and proteomics data collected from the exact same samples and methodology [27]. The MetaboAnalyst 5.0 web-based tool includes the normalization, transformation and scaling of data to complete data integration.

Furthermore, a lipid metabolic network analysis [28] performed with LINEX 2.4.1 webapp to observe functional associations of lipid classes. It computes specific lipid networks based on compounds and lipid classes connections using a lipidomics dataset.

2.7. Extracellular vesicle isolation

EVs were purified from conditioned media of DU145 prostate cancer cell (ATCC, Teddington, UK) grown in Integra bioreactor flasks (Integra Biosciences Corp, Hudson, NH, USA) [24]. EV samples were collected using the sucrose cushion method and resuspended in PBS. Thence, samples were quantified using the BCA-protein assay (Pierce/Thermo, Northumberland, UK), and stored at −80 °C. For treatments of stromal cell cultures, EV were used at 200 μg per mL (approximately equivalent to 1.5 ng per mL of EV-associated TGF-β1) for 72 h.

2.8. Seahorse assay

Oxygen consumption rate and glycolytic activity were assessed using a XF24 Extracellular Flux Analyser (Seahorse Biosciences) to probe O_2 and pH, respectively. Fibroblasts were equilibrated in unbuffered media (60 min at 37 °C in a CO_2-free incubator) prior transfer to the XF24 analyser. For mitochondrial respiration, the oxygen consumption was measured over the assay. First, basal oxygen consumption (OCR) was determined, and then oligomycin (1 μg per ml), FCCP (0.3 μM), FCCP (0.6 μM), and 2 μM rotenone were sequentially injected to assess maximal oxidative capacity, ATP production, coupling efficiency (OCR percentage dedicated to produce ATP) and basal respiration. To analyse glycolytic activity, the extracellular pH was measured over the assay. First, base-line (non-glycolytic) extracellular acidification (ECAR) was determined, and then media alone followed by glucose (10 mM), oligomycin (1 μg per ml), and 2-Deoxyglucose (0.1 M) were sequentially injected to assess maximal glycolytic capacity and glycolysis rate.

Statistical analyses were performed by paired Student's *t*-test using GraphPad PRISM 9.5 software (Graph Pad, San Diego, CA, USA). Each experiment was analysed individually then, the mean ± SEM was represented. All *p*-values lower than 0.05 are considered significant as: * $P > 0.05$, ** $P > 0.01$, *** $P > 0.001$.

3. Results

3.1. CAFs exhibit a differential proteomic, transcriptomic and metabolomics landscapes

In previous studies, we have characterised normal fibroblasts and CAFs derived from the same patient needle biopsies for the typical markers of reactive stroma, α-Smooth Muscle Actin (α-SMA), Cytokeratine, Desmin and Vimentin [7,8,23]. CAFs were not a homogeneous population of myofibroblasts but a heterogenous mixture of fibroblasts at distinct differentiation stages, including a proportion of cells which are α-SMA positive [7]. The normal fibroblasts lacked α-SMA. However, they could be induced to express α-SMA when treated with either soluble or vesicle-associated TGF-β1 [8]. We have previously described a set of proteins that could discriminate CAFs and normal fibroblasts isolated from the patient—matched needle biopsies described in this study [8]. A more recent study [23] identified 19 differentially expressed transcripts that discriminate disease from normal stromal EVs, indicating transcriptional differences between patient samples [23].

The metabolomics study included in this work adds several findings to our published data obtained by proteomics and transcriptomics. The PCA (Fig. S1) showed no explicit distinction between the metabolome of both fibroblast populations. Afterwards, PLS-DA and OPLS-DA models were built by adding group information to metabolomics data of samples. The scores plots are included in Fig. 1A and B, respectively. As it can be observed, a separation tendency was observed in both models mainly through PC1 suggesting distinct metabolite levels in both sample types. Even with this separation tendency, none of the models was validated (CV-ANOVA *p*-value >0.05). Those variables that influence on the most in group separation were selected based on their VIP and p (corr) values. In total 64 and 12 metabolites fulfil VIP >1 and |p(corr)| >0.8 in PLS-DA and OPLS-DA, respectively. In order to select those metabolites of relevant importance, a Venn Diagram including the metabolites was built to select only those metabolites that were identified by both the PLS-DA and OPLS-DA models (Fig. 1C). Relevant metabolites include ceramides (Cer), phosphatidylcholines (PC) and cholesteryl esters (CE) (Table S3).

3.2. Cancer-associated fibroblasts show lipogenic and energy-producing metabolic alterations

The presence of CAFs, with an α-SMA positive myofibroblast-like phenotype, within within the tumour microenvironment is associated with disease progression and poor prognosis. In order to study the metabolic profile of patient-derived CAFs, compared to normal stromal fibroblasts, four platforms based on UPLC-MS were utilised to analyse metabolites. They are fractionated in pools of species with similar

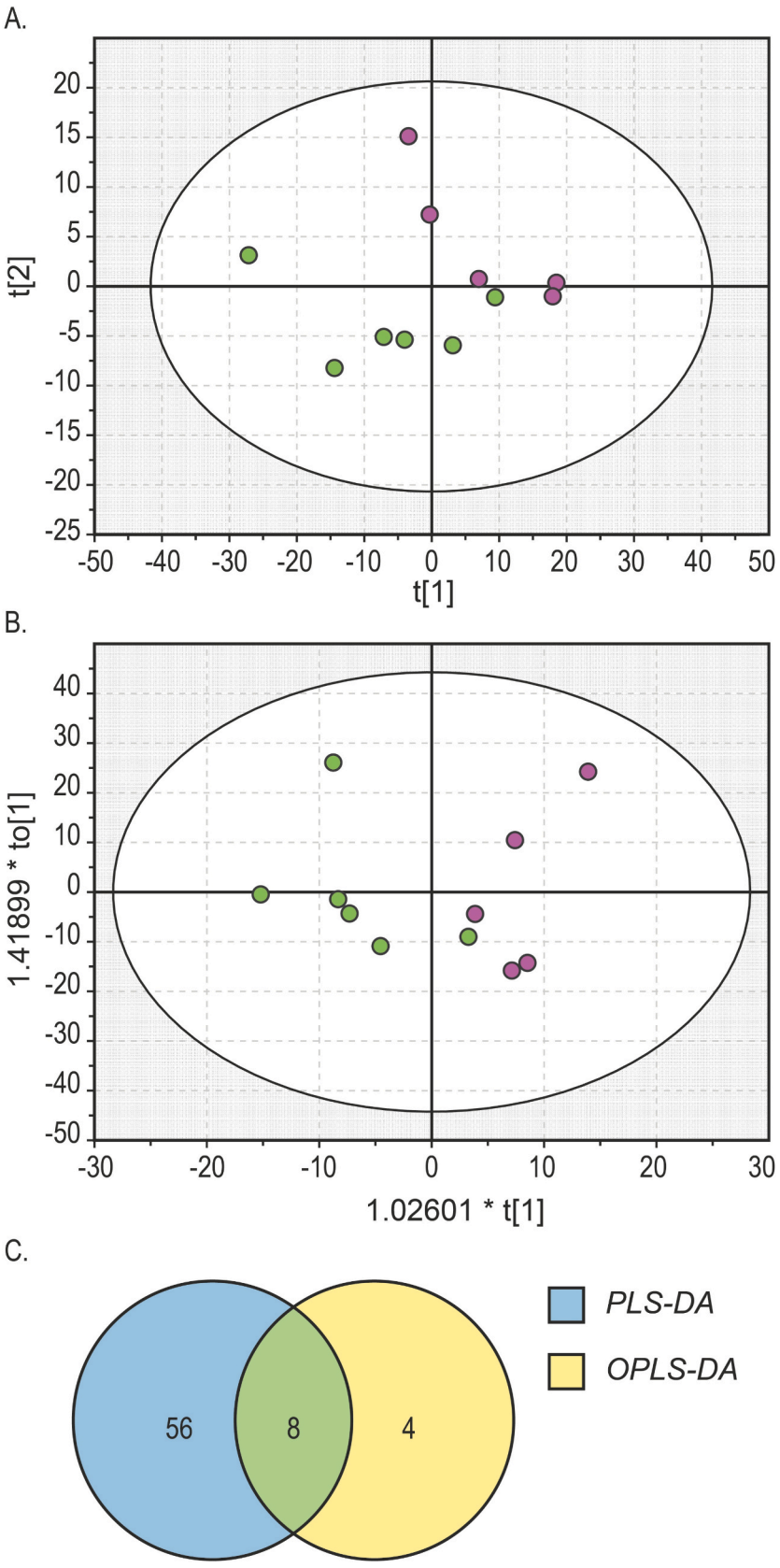

(caption on next page)

Fig. 1. Summary of multivariate metabolomics analysis of normal fibroblasts and CAFs. A. Score scatter plot of the PLS-DA model of fibroblasts obtained from normal and cancer needle biopsies. Model diagnostics (A = 2; R2X = 0.682; R2Y = 0.729; Q2 = 0.337; CV-ANOVA = 0.581). In green, CAF samples and, in purple, normal fibroblasts. B. Score scatter plot of the OPLS-DA model of fibroblasts obtained from normal and cancer needle biopsies. Model diagnostics (A = 2; R2X = 0.682; R2Y = 0.721; Q2 = 0.241; CV-ANOVA = 0.799). In green, CAF samples and, in purple, normal fibroblasts. In green, CAF samples and, in purple, normal fibroblasts. C. Venn diagram of features (metabolites) that influence to the separation of CAF and normal fibroblasts groups in PLS-DA and OPLS-DA models. Results are compiled in Table S3. (For interpretation of the references to colour in this figure legend, the reader is referred to the web version of this article.)

physicochemical properties. The platforms include: (1) Fatty acyls, bile acids, steroids and lysoglycerophospholipids; (2) Glycerolipids, glycerophospholipids, sterol lipids and sphingolipids; (3) Amino acids; (4) Polar metabolites profiling, including central carbon metabolism.

A total of 422 metabolites, of which 47 were significantly at higher levels in CAFs, were identified (Fig. 1A). The volcano plot in Fig. 2A reflects a general trend of raised metabolite levels in CAFs compared to normal fibroblasts. Metabolites showing a significantly different level in disease or normal fibroblasts (p-value<0.05) are compiled in Table S2. Among the significantly more prevalent metabolites, aminoacid tryptophan (Trp) was the only elevated metabolite for a p-value over 0.001. Glutathione (GSH) system was found elevated over 4-fold in cancer, indicating a high detoxification activity, transmembrane transport of organic solutes and/or response to reactive oxygen species [30]. Most of the altered metabolites corresponded to several classes of lipids. To describe metabolic pathways altered in CAFs compared to normal fibroblasts a pathway analysis was computed (Fig. 2B). Indeed, this overrepresentation analysis pinpoints that Trp/Lys/Phe metabolism and GSH system are affected in CAF population. Among lipid pathways, the analysis highlighted steroid biosynthesis, glycerol(phospho)lipid metabolism and linoleic acid (Fatty acids) metabolism. Altogether indicates that CAFs are more active metabolically and exhibit several alterations towards a lipogenic metabolism.

Considering the metabolite class, one can classify families of metabolites that participate in similar metabolic and physiological pathways. In Fig. 3A, a table summarising metabolite class fold changes significant in CAFs is presented. Both analysed polypeptides of central metabolism and, nucleosides and nucleotides were elevated in the cancer group. This could explain a more active state of CAFs compared to normal fibroblasts. Besides, one could observe elevated levels of different types of lipids in cancer samples including cholesteryl esters (CE), n-acyl ethanolamines (NAE), ceramides (Cer) and glycerophospholipids. For this reason, we analysed our quantified set of lipids derived from this metabolomics study to compute lipid associations and visualise important modules of the network (Fig. 3B). The nodes are metabolites and they are connected when they can be readily metabolised between them. In general, there are few clusters of interconnected lipids, which means there are several groups of lipids relevant in CAFs with reasonably different biological function. Considering only significant lipids in the network (Fig. 3A), one can observe that hydroxyeicosapentanoic acids (HEPE) and CE are the most relevant in terms of Fold change in the metabolic network. The accumulation of CE agrees with studies that show an abnormal cholesterol metabolism in cancer [31]. Notably, most elevated CE were those esterified to both

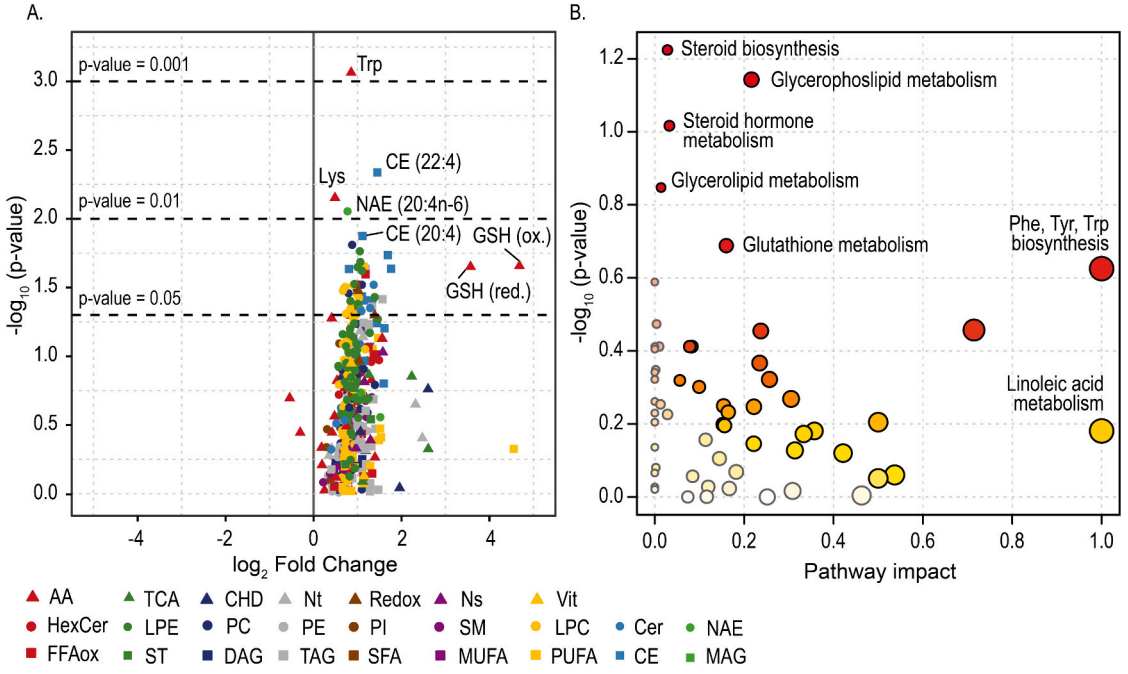

Fig. 2. Summary of metabolomics study (considering individual metabolites) comparing normal and cancer-associated fibroblasts isolated from needle biopsies of radical prostatectomy specimens. A. Volcano plot comparing CAFs and normal fibroblasts as -log10(p-value) against log2(fold change). The different metabolite classes are depicted in different shapes and colours; relevant metabolites are labelled. B. Pathway overrepresentation analysis depicted as –log10 (p-value) against pathway impact. Pathway impact stands for the relative importance of the specific module in the analysed metabolite set. It combines pathway overrepresentation results and centrality measures. Representative pathways were labelled, size of nodes represents pathway impact and their significance ranges from high (in red) towards orange, yellow and white indicating a lower significance. Here, all individual metabolites and their fold changes were considered to rank the enrichment and significance of each pathway. AA: aminoacids; TCA: tricarboxylic acid cycle related metabolites; CHD: Carbohydrates derivatives; Nt: Nucleotides; Redox: electron donor and acceptors; Ns: Nucleosides; Vit: Vitamins; HexCer: Hexosylceramides; LPE: Lysophosphatidylethanolamines; PC: Phosphatidylcholines; PE: Phosphatidylethanolamines; PI: Phosphatidylinositols; SM: Sphingomyelins; LPC: Lysophosphatidylcholines; Cer: Ceramides; NAE: N-acylethanolamines; FFAox: Oxidised fatty acids; ST: Steroids; DAG: Diacylglicerides; TAG: Triacylglicerides; SFA: Saturated fatty acids; MUFA: Monounsaturated fatty acids; PUFA: Polyunsaturated fatty acids; CE: Cholesteryl esters; MAG: Monoacylglicerides. (For interpretation of the references to colour in this figure legend, the reader is referred to the web version of this article.)

A.

Metabolite classification	log_2 FC	p-val
Ceramides	1.01	0.046
Cholesteryl esters	1.53	0.013
Hydroxyeicosapentanoic acids (HEPE)	1.18	0.032
N-acyl ethanolamines	0.91	0.028
Nucleosides and nucleotides	0.95	0.025
Polipeptides of central carbon metabolism	3.50	0.019
Lysophosphatidylcholines	0.78	0.048

B.

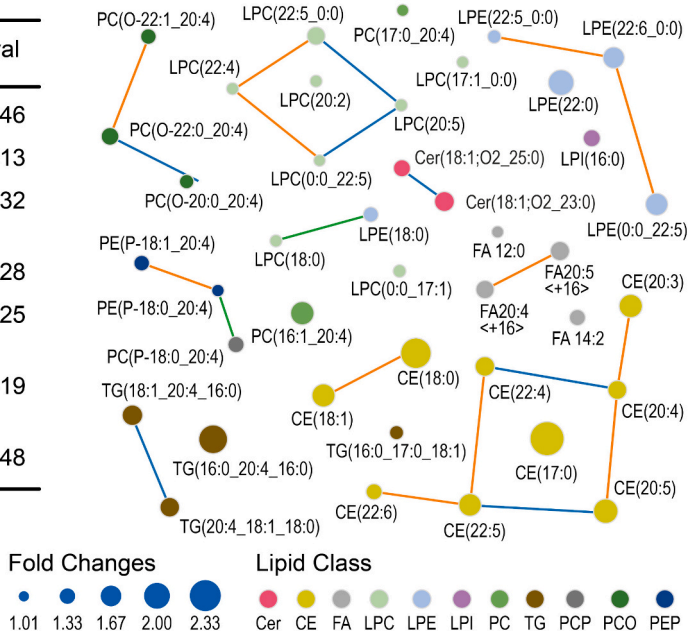

Fig. 3. Summary of metabolomics study (considering metabolites class) comparing normal and cancer-associated fibroblasts isolated from needle biopsies of radical prostatectomy specimens. A. Comparison of metabolic variations between cancer *vs* normal fibroblasts. In this table, the classification of metabolites is considered - metabolites with similar chemical characteristics - instead of comparing each individual metabolite. Fold changes of these paired samples were calculated and the significances of the paired *t*-test are indicated. B. Representation of significant lipid metabolites found in elevated levels in matched-patient samples. Nodes (metabolites) are sized according to their fold change and they are linked according to reaction connection, blue line indicates chain elongation/reduction, green indicates head group modification and, orange indicates saturation/desaturation. Lipid classes are also represented in different colours. Cer: Ceramides; CE: Cholesteryl esters; FA: Fatty acids; LPC: Lysophosphatidylcholines; LPE: Lysophosphatidylethanolamines; LPI: Lysophosphatidylinositols; PC: Phosphatidylcholines; TG: Triacylglicerides; PCP: Ether LPC; PCO: Ether PC; PEP: Ether LPE. (For interpretation of the references to colour in this figure legend, the reader is referred to the web version of this article.)

polyunsaturated 20 and 22 carbon atom of acyl chains (Fig. 3B). Interestingly, HEPE metabolites are oxidised fatty acids (FFAox), associated to fatty acid (FA) mobilisation for energy production in mitochondria. Most of the altered lipids corresponded to glycerophospholipids specifically, lysophosphatidylcholines (LPC) and ether-linked glycerophosphocholines (LPE), which are related to mitochondria well-functioning [32,33]. Anandamine and other NAEs have important anti-inflammatory and anti-cancer properties and, have been associated to inhibition of growth in PCa.

The integration of *omic* approaches often provides a better understanding of physiological outputs. A proteomic study performed by Webber et al. [8] processed the exact same set of patient-matched needle biopsies utilised in this study. As samples underwent the same experimental procedures, the integration of proteomics and metabolomics data may reveal relevant metabolic flux distributions. In Fig. 4 one can observe a joint-pathway analysis that combines significant variations of the proteome and metabolome comparing CAFs against normal fibroblasts. This analysis computed by Metaboanalyst provides the most relevant (*p*-value) and affected (Pathway impact) metabolic pathways. This integrated metabolic pathway analysis confirms the rewire of CAFs towards lipogenic metabolism since glycerophospholipid, arachidonic acid, linoleic acid and fatty acid metabolism were highlighted in CAFs (Fig. 4). Moreover, the fact aminoacyl t-RNA biosynthesis was over-represented proposes the elevated levels of aminoacids, nucleosides and nucleotides are related to a higher transcriptomic activity of CAFs. This phenotype is characteristic of cancer-associated tissues [34,35]. Interestingly, it is suggested that glycolysis/gluconeogenesis and pentose phosphate pathways are also over-represented. This feature is also characteristic of highly proliferative cells or tissues, however, there were no significant differences detected in metabolites of those pathways. Hence, it suggests the main central metabolism modifications are described by proteomics data.

3.3. Treatment with EVs modifies basal respiration of normal fibroblasts to a CAF-like phenotype

In previous studies with the same treatments and sample preparations, we have shown TGF-β1 associated to EVs was required to induce myofibroblast differentiation of normal fibroblasts, resulting in angiogenic and tumour-promoting characteristics [7]. Also, a proteomics study comparing EV-generated myofibroblasts and those naturally arising *in situ* confirmed their similarity [8]. The activation of myofibroblast-rich stroma is considered by some as a rate-limiting step, essential for cancer progression [7]. Thus, one could expect that the metabolism of normal fibroblast show alterations upon their treatment with EVs.

For this reason, we have performed glycolytic and mitochondrial stress assays on normal- and disease-derived stromal fibroblasts and also, to normal fibroblasts incubated with soluble TGF-β1 (sTGF-β1) or DU145-derived EVs. Extracellular acidification rate (ECAR) in response to glucose, oligomycin (ATP synthesis inhibitor) and 2-DG (glycolysis inhibitor) was plotted over time to study the glycolytic rate of fibroblasts (Fig. S2). Glucose is taken up by the cells and converted to lactate, generating ATP and protons (Fig. S3A). Glycolysis rate do not show a distinctive phenotype when comparing normal fibroblasts to CAFs. Oligomycin was used to inhibit mitochondrial ATP production, shifting energy production to glycolysis, thus revealing the maximal glycolytic capacity of fibroblasts (Fig. S3B). The difference between glycolytic capacity and basal glycolysis rate was defined as the glycolytic reserve (Fig. S3C). The fact glycolytic reserve is neither distinctive comparing normal fibroblasts to CAFs but its value is over 100 % suggests that fibroblasts do not uniquely rely on glycolysis to obtain energy. In summary, no significant differences were measured between normal and disease fibroblasts nor upon TGF-β1 or EV treatment regarding their use of glucose to produce energy. The fact no significant differences were

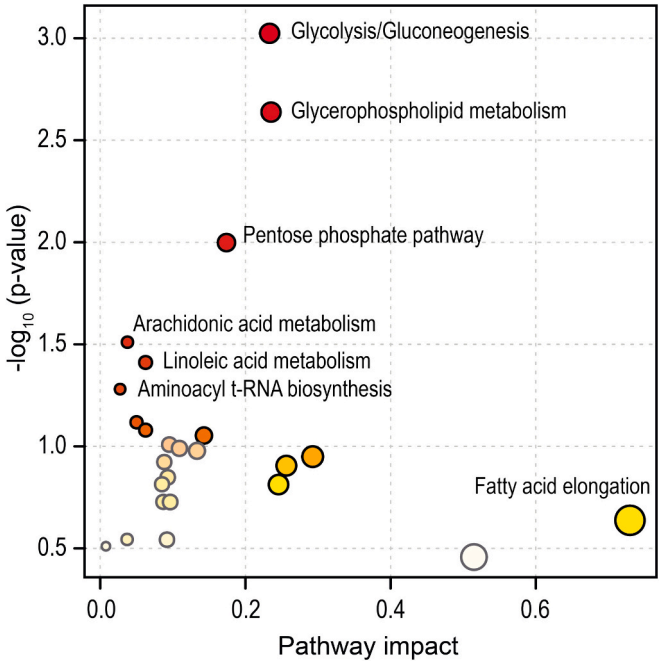

Fig. 4. Joint-pathway analysis of significant proteins and metabolites differentially quantified in patient-matched normal and cancer-associated stromal fibroblasts. Pathway overrepresentation analysis is depicted as –log10 (*p*-value) against pathway impact Pathway impact stands for the relative importance of the specific module in the analysed metabolite set. It combines pathway overrepresentation results and centrality measures. Representative pathways were labelled, size of nodes represents pathway impact and their significance ranges from high (in red) towards orange, yellow and white indicating a lower significance. (For interpretation of the references to colour in this figure legend, the reader is referred to the web version of this article.)

described in metabolomics study suggests that the typical glycolytic phenotype of PCa is not readily described in stromal cells.

To study mitochondrial metabolism, oxygen consumption rate (OCR) in response to oligomycin (ATP coupler), FCCP (an electron transport chain accelerator), and rotenone (mitochondrial inhibitor) was plotted over time (Fig. S4). Oligomycin inhibits ATP synthesis, so it is utilised to describe the oxygen consumption devoted to ATP synthesis (Fig. 5A) so the coupling efficiency, percentage of mitochondrial respiration for ATP production, could be calculated (Fig. 5C). In Fig. 5B the contribution of basal respiration and reserve capacity (%) is depicted. In general, both basal respiration and ATP production associated to mitochondria tend to increase in CAFs. Moreover, treatment with soluble TGF-β1 or PCa-derived EVs significantly increased basal respiration after 72 h incubation. This result suggests normal fibroblasts increased their mitochondrial metabolism with these treatments.

4. Discussion

The onset of a reactive stroma and the emergence of CAF phenotypes is a feature comprehensively studied in solid cancers including PCa [6–8,23,36]. Other PCa reports often compare metabolic alterations between different types of tissues or between low and high grade of disease. In this line, a study using mass spectrometry imaging (MSI) distinguished prostate compartments as well as disease stages in prostate slices from patients. This MSI approach described a distinctive metabolism of prostate stroma and epithelium regions as well as between non-cancerous and cancerous epithelium [11]. Many studies evaluated the interaction of PCa with reactive stroma [2,12–17], however, very few describe metabolite levels across different types of stroma [12].

Previous reports using the exact same set of matched-patient stroma biopsies confirmed the existence of myofibroblast-like cells within diseased regions of the tissue, by positive staining of both α-SMA, and vimentin, and lack of expression of desmin or the cytokeratins [7,8,23]. Upon stimulation with (soluble or EV-associated TGF-β1, differentiation of normal tissue-derived fibroblasts into myofibroblasts was verified by the onset of α-SMA expression [8]. Nonetheless, the cancer-associated stroma was a mixture of varying proportions of fibroblasts and myofibroblasts-like cells [29,37]. One can expect that although such heterogeneity is an important factor in promoting tumour growth it may well hinder our capacity to fully appreciate metabolic alterations that arise in CAFs. This metabolomics study has identified some altered metabolites and metabolic pathways; however, it could not definitively

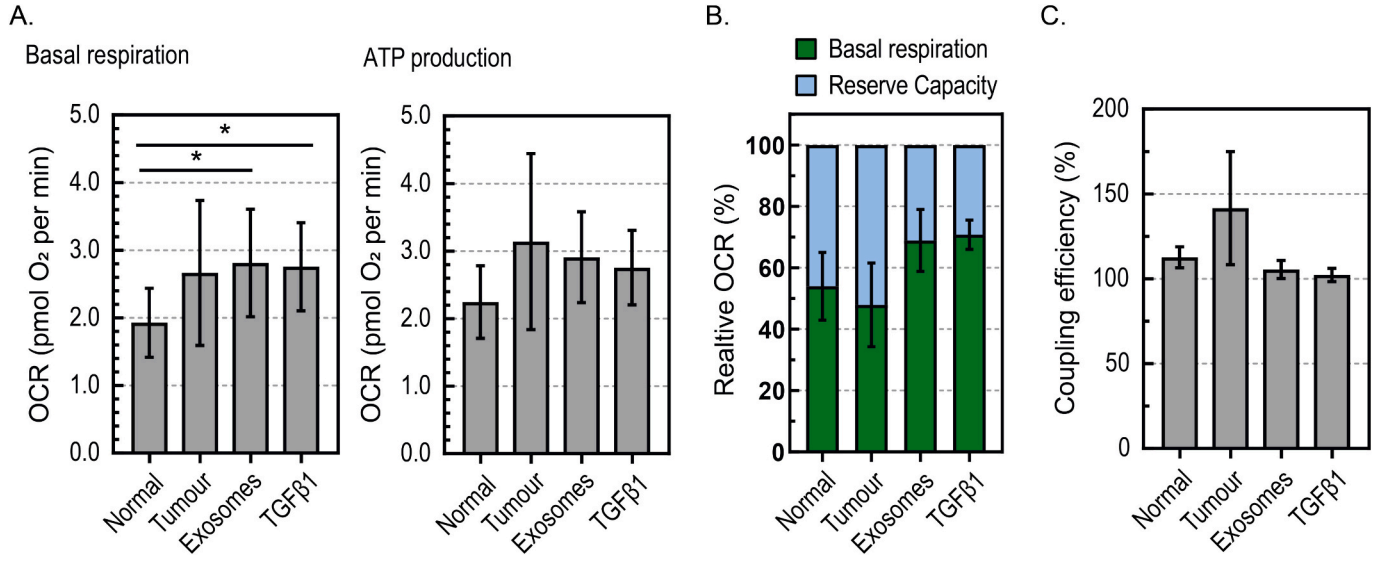

Fig. 5. Analysis of mitochondrial stress assay comparing untreated normal- and cancer-associated stromal fibroblasts (tumour), or normal fibroblasts pre-treated with either exosomes or TGF-β1 (data in Fig. S4). A. OCR relating to basal respiration and specifically to ATP production (mean ± SEM; $n = 6$) was calculated. B. Maximal OCR was established as 100 % and OCR apportioned between basal respiration and reserve capacity represented C. Reserve capacity expressed as percentage of basal respiration was calculated (mean ± SEM; n = 6) and the efficiency of basal respiration towards ATP production was represented (mean ± SEM; n = 6), as coupling efficiency.

distinguish stromal CAFs from normal fibroblasts using a non-supervised PCA approach. Besides, adding information about class, a clear tendency was observed in both PLS-DA and OPLS-DA models. Even no significant model was generated; important metabolites were obtained from multivariate analysis that matches with univariate analysis. This highlighted the importance of these metabolites – CE (20:5), Cer (d18:1/25:0), PC (O-22:1/20:4) and PC (P-18:0/20:4) - involved in lipid biosynthesis pathways and pointed them out for further studies with more samples and individuals. The lack of clear significant results could be due to CAF heterogeneity and a limited number of samples. Moreover, one should be aware that prior frozen samples can influence metabolomics analyses when they are not well prepared since protein content could affect metabolite recoveries. As in this analysis all samples underwent the same procedures, the output will not change.

In this manuscript, we present metabolomics data comparing normal and cancer-associated fibroblasts (CAFs) from the same patient which is, to our knowledge, the first such exploration. Our multiplatform analysis established elevated levels of several metabolic classes in CAFs. The increment of cholesteryl esters has been already observed in other studies concerning tumour cell lines and samples [31,38], which is on agreement with the upregulated tendency observed (see Fig. 3). Actually, cells make reservoirs of cholesteryl ester that can be transferred to nearby or even distal cells [39]. This might well be the reason myofibroblasts accumulate lipids. Seeking for energy sources, epithelial cancer cells undergo a characteristic rewiring of their metabolism from an extremely unproductive secretion of citric acid to a closed TCA cycle with an elevated mitochondrial respiration. Besides, this rewiring is accompanied with the uptake of circulating lipids [40,41] as well as translocation of lipids from adipocytes [42]. As they consume lipids and specifically, cholesteryl esters [38], supportive CAFs could be fuelling either themselves with these compounds, nearby cancer cells or both. Interestingly, CAFs seem to mobilise *de novo* free fatty acids as energy source; oxidised fatty acid species as HEPE were elevated in cancer-associated fibroblasts. Altogether indicates a consumption of newly built lipids to fuel themselves while building up cholesteryl esters reservoirs, which are easily transported and readily available to transfer it between cells. The fact acyclglycerols were not accumulated in CAFs, although few triacyclglycerols were increased and, acetyl-CoA shows a quite high fold change (Table S2) hints that myofibroblasts preferentially store energy as cholesteryl ester compounds while the oxidation of free fatty acids satisfy their energy needs.

The higher metabolic activity suggested by an over-representation of mostly all metabolites measured in this study is further confirmed with elevated levels of nucleosides and nucleotides. When proteomics data is considered the biosynthesis of tRNA aminoacyls is highlighted, which indicates a higher transcriptional and translational activities. Specifically, the increment of NAD suggests a mobilisation of fibroblast reducing power to generate energy in mitochondria or fuel anabolic reactions. Moreover, accumulation of ceramides has been comprehensively related to cell differentiation, arrest of cell cycle and apoptosis [43–45]. This class, and concretely Cer(d18:1/25:0), followed the described tendency (see Fig. 3, Table S2 and S3). Newly differentiated fibroblasts exhibit higher levels of ceramides and possibly, apoptotic mechanisms are counteracted by other compounds as anandamide. Anandamide is an endocannabinoid - detected in higher levels in CAFs - with important anti-inflammatory and anti-cancer properties [46] that demonstrated inhibition of growth in transformed cell lines from human prostate [47,48].

Our previous proteomics comparison of normal fibroblasts and CAFs revealed distinct differences between the two populations [8]. Furthermore, several differences were observed in response to specific treatments with either sTGF-β1 or EV-associated TGF-β1. For instance, they described a higher presence of Annexin-I, which has a role in regulating VEGF function, in CAFs as well as altered mitochondrial proteins, linking CAFs to mitochondrial rearrangement. In this manuscript, we approached the assessment of metabolic alterations upon sTGF-β1 or EV-associated TGF-β1 treatments by Seahorse stress assays. Even considering the limitation of such assays, where O_2 consumption and pH acidification are recorded over time, the glycolytic rate and oxidative mitochondrial activity of cells was assessed. ECAR informs that glycolytic activity associated to CAFs was not increased. This, together with the fact that the integration of proteomics and metabolomics indicates an alteration in central metabolism, suggests that these pathways were not used in the catabolic but in the anabolic direction. Only basal respiration, in the mitochondrial stress assay, was distinctive when comparing between CAFs and normal fibroblasts. Moreover, the treatment with sTGF-β1 and EVs containing TGF-β1 showed a similar outcome. This result links the distinctive metabolic profile to mitochondrial metabolism. An increased GSH is usually correlated to the presence of ROS due to mitochondrial activity while altered levels of FFAox may indicate the burning of lipids in mitochondria seeking for energy and counteracting ROS. Perhaps a longer stimulation or a higher dose of sTGF-β1 or EVs is required to observe further metabolic alterations associated to cancer in normal fibroblasts. Nonetheless, this data hints that metabolic rewiring is related to an altered metabolism of mitochondria, yet the specific role of cancer-associated EVs and the metabolic mechanisms in stromal differentiation and shift towards its reactive state require further evaluation.

A limitation of this study has been the arguably low number of samples available for metabolomics. In contrast, the strength is the collection of donor matched-paired biopsy samples that reflect healthy and disease tissue regions of stroma from the same patient. This type of data draws relevant conclusions of processes and alterations occurring in each patient. Even so, the outcome of this study described metabolic differences with sparse impact in the entire metabolome. Once combined with proteomics data from the exact same set of samples, the outcome acquired a higher relevance in determining important metabolic processes driving myofibroblast differentiation. The integration of significant proteins and metabolites differentially measured in normal and cancer fibroblasts confirmed a major alteration in lipid metabolism. A variation of glycerophospolipids indicates an enrichment of the major membrane type of lipids. Interestingly, this type of lipids have been associated to mitochondria dynamics and well-functioning [32,33]. Although lipids can participate in signalling processes or be used as building blocks, in this study most metabolic alterations point out fuelling or energy storage processes. Major free fatty acid pathways – linoleic and arachidonic - are altered together with an accumulation of cholesteryl esters and few oxidised fatty acids. This indicates a mobilisation of lipids to produce energy but also the production of lipid reservoirs readily available for transport. Moreover, central metabolism pathways – glycolysis/gluconeogenesis and pentose phosphate - are positively altered in CAFs only including the proteome to the analysis. This suggests that as protein queries were the most prominent and overlapped a higher number of pathways compared to metabolites, the output of this integrative analysis could be determined majorly by differences in the proteome.

5. Conclusions

The phenotype of cancer-associated stroma is characteristic and diverge from healthy stroma at both transcriptional and proteomic level. In this manuscript, we discussed metabolic differences measured in patient-matched normal and tumour fibroblasts from prostate adjacent regions. This approach has no precedents in literature. A multiplatform metabolomics analysis of these fibroblasts determined an increased metabolic activity of CAFs. Also, many lipid classes were altered, indicating an enhanced lipogenic metabolism. Lipid reservoir species as cholesteryl ester were measured in CAFs together with building block compounds as lysophosphatidylcholines. Furthermore, alterations in GSH system and oxidised fatty acids suggests the involvement of mitochondria in CAF distinct metabolism. Herewith, this integrated study points out lipogenic pathways and a modified mitochondrial

metabolism to be relevant during fibroblast differentiation.

Previous studies demonstrated the treatment with TGF-β1 or TGF-β1-EVs provoke a response in normal fibroblasts towards myofibroblasts. Thence, we assessed whether EVs containing TGF-β1 or soluble TGF-β1 could trigger a metabolic response in normal fibroblasts. Often, in such differentiation processes, cells desperately look for new energy sources and building blocks in order to sustain growth. According to our metabolomics and Seahorse data, the alternative pathway to obtain energy is not glycolysis. Moreover, Seahorse data shows that basal respiration associated to mitochondria was increased in CAFs so as normal fibroblasts upon TGF-β1 or EV stimulation. In conclusion, one can propose the altered metabolism of tumour-associated fibroblasts is driven by an oxygen-dependent metabolism associated to mitochondria. The metabolic status of normal fibroblasts is altered upon EV (and TGF-β1) stimulation and it is associated to mitochondria metabolism.

Funding sources

The authors of this study were supported by funds from the European Union's Horizon 2020 Research and Innovation Programme under grant agreement no. 860303. European Union also funded this work with two Horizon grant agreements, no. 101079264 and no. 101095679. The study was also supported from a Cancer Research Wales Programme Grant. The European Network on Microvesicles and Exosomes in Health and Disease (ME-HAD) with the cost action STSM-BM1202 under grant number 190514-044080 financed a Short-Term Scientific Mission of J. W.

CRediT authorship contribution statement

Guillermo Bordanaba-Florit: Writing – review & editing, Writing – original draft, Visualization, Formal analysis, Data curation. **Félix Royo:** Writing – review & editing, Methodology, Investigation. **Oihane E. Albóniga:** Writing – review & editing, Supervision. **Aled Clayton:** Writing – review & editing, Supervision, Project administration, Funding acquisition, Conceptualization. **Juan Manuel Falcón-Pérez:** Writing – review & editing, Supervision, Project administration, Funding acquisition, Conceptualization. **Jason Webber:** Writing – review & editing, Resources, Methodology, Investigation, Funding acquisition, Conceptualization.

Declaration of competing interest

The authors declare that they have no known competing financial interests or personal relationships that could have appeared to influence the work reported in this paper.

Data availability

Data will be made available on request.

Acknowledgements

We thank the Exosomes lab and Metabolomics Platform staff at CIC bioGUNE for experiment assistance and guidance. We would like to thank OWL metabolomics for performing the metabolomics assay and statistical analysis of prostatic human fibroblast samples.

Appendix A. Supplementary data

Supplementary data to this article can be found online at https://doi.org/10.1016/j.bbadis.2024.167229.

References

[1] M. El-Alfy, G. Pelletier, L.S. Hermo, F. Labrie, Unique features of the basal cells of human prostate epithelium, Microsc. Res. Tech. 51 (2000) 436–446.
[2] D.A. Barron, D.R. Rowley, The reactive stroma microenvironment and prostate cancer progression, Endocr. Relat. Cancer 19 (2012) 187–204.
[3] M.B. Tessem, et al., A balanced tissue composition reveals new metabolic and gene expression markers in prostate cancer, PloS One 11 (2016) 1–15.
[4] N. Yanagisawa, et al., Stromogenic prostatic carcinoma pattern (carcinomas with reactive stromal grade 3) in needle biopsies predicts biochemical recurrence-free survival in patients after radical prostatectomy, Hum. Pathol. 38 (2007) 1611–1620.
[5] Y. Kojima, et al., Autocrine TGF-β and stromal cell-derived factor-1 (SDF-1) signaling drives the evolution of tumor-promoting mammary stromal myofibroblasts, Proc. Natl. Acad. Sci. U. S. A. 107 (2010) 20009–20014.
[6] J. Webber, R. Steadman, M.D. Mason, Z. Tabi, A. Clayton, Cancer exosomes trigger fibroblast to myofibroblast differentiation, Cancer Res. 70 (2010) 9621–9630.
[7] J.P. Webber, et al., Differentiation of tumour-promoting stromal myofibroblasts by cancer exosomes, Oncogene 34 (2015) 319–333.
[8] J.P. Webber, et al., Prostate stromal cell proteomics analysis discriminates normal from tumour reactive stromal phenotypes, Oncotarget 7 (2016) 20124–20139.
[9] M.K. Andersen, G.F. Giskeødegård, M.B. Tessem, Metabolic alterations in tissues and biofluids of patients with prostate cancer, Curr Opin Endocr Metab Res 10 (2020) 23–28.
[10] D. Hanahan, R.A. Weinberg, Hallmarks of cancer: the next generation, Cell 144 (2011) 646–674.
[11] M.K. Andersen, et al., Spatial differentiation of metabolism in prostate cancer tissue by MALDI-TOF MSI, Cancer Metab 9 (2021) 1–13.
[12] M.K. Andersen, et al., Integrative metabolic and transcriptomic profiling of prostate cancer tissue containing reactive stroma, Sci. Rep. 8 (2018) 1–11.
[13] J.L. Carstens, et al., FGFR1-WNT-TGF-β signaling in prostate cancer mouse models recapitulates human reactive stroma, Cancer Res. 74 (2014) 609–620.
[14] A. Giatromanolaki, M.I. Koukourakis, A. Koutsopoulos, S. Mendrinos, E. Sivridis, The metabolic interactions between tumor cells and tumor-associated stroma (TAS) in prostatic cancer, Cancer Biol. Ther. 13 (2012) 1284–1289.
[15] S. Tyekucheva, et al., Stromal and epithelial transcriptional map of initiation progression and metastatic potential of human prostate cancer, Nat. Commun. 8 (2017) 1–10.
[16] Z. Frankenstein, et al., Stromal reactivity differentially drives tumour cell evolution and prostate cancer progression, Nat Ecol Evol 4 (2020) 870–884.
[17] Z. Richards, et al., Prostate stroma increases the viability and maintains the branching phenotype of human prostate organoids, iScience 12 (2019) 304–317.
[18] I. Nazarenko, et al., Cell surface tetraspanin Tspan8 contributes to molecular pathways of exosome-induced endothelial cell activation, Cancer Res. 70 (2010) 1668–1678.
[19] J.L. Hood, H. Pan, G.M. Lanza, S.A. Wickline, Paracrine induction of endothelium by tumor exosomes, Lab. Invest. 89 (2009) 1317–1328.
[20] A. Ramteke, et al., Exosomes secreted under hypoxia enhance invasiveness and stemness of prostate cancer cells by targeting adherens junction molecules, Mol. Carcinog. 54 (2015) 554–565.
[21] S. Josson, et al., Stromal fibroblast-derived miR-409 promotes epithelial-to-mesenchymal transition and prostate tumorigenesis, Oncogene 34 (2015) 2690–2699.
[22] V.R. Minciacchi, et al., MYC mediates large oncosome-induced fibroblast reprogramming in prostate cancer, Cancer Res. 77 (2017) 2306–2317.
[23] A.P. Shephard, et al., Stroma-derived extracellular vesicle mRNA signatures inform histological nature of prostate cancer, J Extracell Vesicles 10 (2021).
[24] J.P. Mitchell, J. Court, M.D. Mason, S. Tabi, A. Clayton, Increased exosome production from tumour cell cultures using the Integra CELLine culture system, J. Immunol. Methods 335 (2008) 98–105.
[25] F.M. van der Kloet, I. Bobeldijk, E.R. Verheij, R.H. Jellema, Analytical error reduction using single point calibration for accurate and precise metabolomic phenotyping, J. Proteome Res. 8 (2009) 5132–5141.
[26] L.E. Moses, Matched pairs *t* -tests, in: Encyclopedia of Statistical Sciences, John Wiley & Sons, Inc., Hoboken, NJ, USA, 2006, https://doi.org/10.1002/0471667196.ess1551.pub2.
[27] Z. Pang, et al., MetaboAnalyst 5.0: narrowing the gap between raw spectra and functional insights, Nucleic Acids Res. 49 (2021) W388–W396.
[28] N. Köhler, T.D. Rose, L. Falk, J.K. Pauling, Investigating global Lipidome alterations with the lipid network explorer, Metabolites 11 (2021) 488.
[29] J.A. Tuxhorn, G.E. Ayala, D.R. Rowley, Reactive stroma in prostate cancer progression, J. Urol. 166 (2001) 2472–2483.
[30] H. Jefferies, et al., Glutathione, ANZ J. Surg. 73 (2003) 517–522.
[31] M.R. Tosi, V. Tugnoli, Cholesteryl esters in malignancy, Clin. Chim. Acta 359 (2005) 27–45.
[32] S.E. Horvath, G. Daum, Lipids of mitochondria, Prog. Lipid Res. 52 (2013) 590–614.
[33] K. Funai, S.A. Summers, J. Rutter, Reign in the membrane: how common lipids govern mitochondrial function, Curr. Opin. Cell Biol. 63 (2020) 162–173.
[34] J.S. Owen, A. Clayton, H.B. Pearson, Cancer-associated fibroblast heterogeneity, activation and function: implications for prostate cancer, Biomolecules 13 (2022) 67.
[35] R. Melchionna, P. Trono, A. Di Carlo, F. Di Modugno, P. Nisticò, Transcription factors in fibroblast plasticity and CAF heterogeneity, J. Exp. Clin. Cancer Res. 42 (2023) 347.

[36] J. Webber, V. Yeung, A. Clayton, Extracellular vesicles as modulators of the cancer microenvironment, Semin. Cell Dev. Biol. 40 (2015) 27–34.
[37] O.E. Franco, et al., Altered TGF-β Signalling in a subpopulation of human stromal cells promotes prostatic carcinogenesis, Cancer Res. 71 (2011) 1272–1281.
[38] S. Yue, et al., Cholesteryl Ester accumulation induced by PTEN loss and PI3K/AKT activation underlies human prostate Cancer aggressiveness, Cell Metab. 19 (2014) 393–406.
[39] L. Galbraith, H.Y. Leung, I. Ahmad, Lipid pathway deregulation in advanced prostate cancer, Pharmacol. Res. 131 (2018) 177–184.
[40] X. Wu, G. Daniels, P. Lee, M.E. Monaco, Lipid metabolism in prostate cancer, Am J Clin Exp Urol 2 (2014) 111–120.
[41] N.B. Kuemmerle, et al., Lipoprotein lipase links dietary fat to solid tumor cell proliferation, Mol. Cancer Ther. 10 (2011) 427–436.
[42] E. Gazi, et al., Direct evidence of lipid translocation between adipocytes and prostate cancer cells with imaging FTIR microspectroscopy, J. Lipid Res. 48 (2007) 1846–1856.
[43] F. Condorelli, P.L. Canonico, M.A. Sortino, Distinct effects of ceramide-generating pathways in prostate adenocarcinoma cells, Br. J. Pharmacol. 127 (1999) 75–84.
[44] F. Fiorani, et al., Ceramide releases exosomes with a specific miRNA signature for cell differentiation, Sci. Rep. 13 (2023) 10993.
[45] K. Kimura, M. Markowski, L.C. Edsall, S. Spiegel, E.P. Gelmann, Role of ceramide in mediating apoptosis of irradiated LNCaP prostate cancer cells, Cell Death Differ. 10 (2003) 240–248.
[46] L. De Petrocellis, et al., The endogenous cannabinoid anandamide inhibits human breast cancer cell proliferation, Proc. Natl. Acad. Sci. 95 (1998) 8375–8380.
[47] P.C. Schmid, L.E. Wold, R.J. Krebsbach, E.V. Berdyshev, H.H.O. Schmid, Anandamide and other *N* -acylethanolamines in human tumors, Lipids 37 (2002) 907–912.
[48] M. Mimeault, N. Pommery, N. Wattez, C. Bailly, J.-P. Hénichart, Anti-proliferative and apoptotic effects of anandamide in human prostatic cancer cell lines: implication of epidermal growth factor receptor down-regulation and ceramide production, Prostate 56 (2003) 1–12.